Applied Physics Letters

Flexible spin-orbit torque devices

Cite as: Appl. Phys. Lett. **107**, 252401 (2015); https://doi.org/10.1063/1.4936934
Submitted: 13 September 2015 • Accepted: 20 November 2015 • Published Online: 21 December 2015

OukJae Lee, Long You, Jaewon Jang, et al.

ARTICLES YOU MAY BE INTERESTED IN

Spin-orbit torques: Materials, physics, and devices
Applied Physics Letters **118**, 120502 (2021); https://doi.org/10.1063/5.0039147

Spin transfer torque devices utilizing the giant spin Hall effect of tungsten
Applied Physics Letters **101**, 122404 (2012); https://doi.org/10.1063/1.4753947

Recent advances in spin-orbit torques: Moving towards device applications
Applied Physics Reviews **5**, 031107 (2018); https://doi.org/10.1063/1.5041793

AIP Publishing

© 2015 AIP Publishing LLC.

Flexible spin-orbit torque devices

OukJae Lee,[1] Long You,[1] Jaewon Jang,[1] Vivek Subramanian,[1] and Sayeef Salahuddin[1,2]
[1]Department of Electrical Engineering and Computer Sciences, University of California at Berkeley, Berkeley, California 94720, USA
[2]Materials Sciences Division, Lawrence Berkeley National Laboratory, Berkeley, California 94720, USA

(Received 13 September 2015; accepted 20 November 2015; published online 21 December 2015)

We report on state-of-the-art spintronic devices synthesized and fabricated directly on a flexible organic substrate. Large perpendicular magnetic anisotropy was achieved in ultrathin ferromagnetic heterostructures of Pt/Co/MgO sputtered on a non-rigid plastic substrate at room temperature. Subsequently, a full magnetic reversal of the Co was observed by exploiting the spin orbit coupling in Pt that leads to a spin accumulation at the Pt/Co interface when an in-plane current is applied. Quasi-static measurements show the potential for operating these devices at nano-second speeds. Importantly, the behavior of the devices remained unchanged under varying bending conditions (up to a bending radius of $\approx \pm 20$–30 mm). Furthermore, the devices showed robust operation even after application of 10^6 successive pulses, which is likely sufficient for many flexible applications. Thus, this work demonstrates the potential for integrating high performance spintronic devices on flexible substrates, which could lead to many applications ranging from flexible non-volatile magnetic memory to local magnetic resonance imaging. © *2015 AIP Publishing LLC*.
[http://dx.doi.org/10.1063/1.4936934]

Electronic devices that can be integrated with soft, curvilinear, and time-varying surfaces form the basis of many emerging technologies such as paper-like displays, solar cells, electronic eyes, synthetic sensitive skins, health monitoring devices, etc.[1–4] Recognizing this opportunity, there have been recent efforts to integrate spin-based technologies onto flexible substrates. For example, magnetic films with in-plane anisotropy (IPA) were synthesized on various types of plastic substrates for studying giant strain effects.[5–8] Recently, flexible magnetic sensors have been demonstrated utilizing giant magnetoresistance or tunneling magnetoresistance effects.[3,9,10] However, integration of high performance devices that take advantage of recent discoveries[11–15] in spintronics, such as ultra-thin ferromagnetic films with perpendicular magnetic anisotropy (PMA),[13] current induced excitation of magnetization exploiting spin transfer torque,[11,12,14] nanosecond magnetization dynamics, etc., are yet to be reported on a *flexible* platform.

In this paper, we present a demonstration of in-plane current induced switching of magnetization in a perpendicularly polarized Pt/Co/MgO dot by directly synthesizing the heterostructures on a flexible substrate at room temperature. The switching exploits the recently discovered spin orbit coupling (SOC) mediated spin accumulation at the Co/Pt interface, which exerts a torque on the Co magnetization.[12,16–19] Henceforth, we shall call this mechanism spin-orbit torque (SOT).[20–25] The fabricated devices exhibit fully deterministic magnetic reversals when the direction of the in-plane current is reversed. The switching is demonstrated for both direct current and pulsed voltages of 10 ns pulse-width. We further show that the operation is robust after millions of successive operations, and that the magnetic and electric characteristics of the devices remain stable for both compressive and tensile strain conditions up to a radius (R) of curvature $\approx$20–30 mm, corresponding to 0.2%–0.3% strain (ε).[26] Note that this range of strain is sufficient for most roll-to-roll manufacturing tools used for flexible electronics.[27] Therefore, our work indicates that the entire suite of cutting-edge spintronic/nanomagnetic devices can, in principle, be integrated with a flexible platform.

Ultrathin multilayer films were deposited on a flexible plastic substrate and for reference on a rigid thermally oxidized Si substrate (Si/SiO_x) at room temperature using dc/rf magnetron sputtering. The multilayers consisted of substrate/Ta(1)/Pt(5)/Co(t_{Co})/ MgO(2)/Ta(2) (thickness in nm) where the thickness of cobalt (t_{Co}) was varied from 0.6 to 2.0 nm. We used a polyethylene naphthalate substrate coated with a planarizing polymer layer (PENC) as a flexible plastic substrate[28] for several reasons. First, PENC has a very low surface roughness ($R_a \approx 0.6$–0.7 nm) that is comparable to the R_a ($\approx$0.4–0.5 nm) of the Si/SiO_x. The R_a of the PENC satisfies a necessary condition for the ultrathin magnetic layer to be continuous so as to have sufficient interfacial anisotropy energy. Second, our tests showed that the sputtered films on the PENC were neither detached nor cracked during the lithography process, but that other substrates we tried were problematic in the adhesion or in the growth of the films. Notably, our as-grown films with 1 nm of Ta buffer layer on the PENC had sufficient PMA; thus, further post-annealing was not performed. The ability to obtain good PMA without annealing was critical due to the limitations of the plastic substrate in general in terms of process temperature. For example, the PENC will be melted at the elevated temperature (T) if $T > T_m$ ($\approx$263 °C), e.g., 300–400 °C, a range of temperature that is widely used for the enhancement of PMA at the interface of Pt/Co.[16–18]

We measured the magnetic anisotropies of the films on the PENC as a function of the t_{Co} (0.6–2.0 nm). We observed a strong out-of-plane anisotropy (OPA) for the film with $t_{Co} \approx 1.0$ nm and an IPA for the one with $t_{Co} \approx 2.0$ nm. There

 © 2015 AIP Publishing LLC

was an anisotropy transition between OPA and IPA at around $t_{Co} \approx 1.6$–1.7 nm. The results clearly show that the interfacial anisotropy energy[13] gives a strong PMA similar to that observed in the multilayer structures on the conventional Si/SiO$_x$. Based on the measured magnetic properties, we determined the saturation magnetization of the Co $(M_s) \approx 970\,\text{emu/cm}^3$, the interfacial anisotropy energy density $(K_s) \approx 2.67\,\text{erg/cm}^2$, the volume anisotropy energy density $(K_v) \approx -1.04 \times 10^7\,\text{erg/cm}^3$, and the magnetostriction of the Co $(\lambda_{Co}) \approx -1 \times 10^{-5}$. Interestingly, we observed that a tensile strain $(\varepsilon > 0)$ enhanced PMA of the Pt/Co films while a compressive strain $(\varepsilon < 0)$ reduced PMA. This is due to the *negative* sign of λ_{Co} because the effective magnetic anisotropy energy with an in-plane strain (ε) becomes $K_{eff}(\varepsilon) = K_{eff} - 3\lambda_{Co}Y_{Co}\varepsilon/2$, where $H_k^{eff}(\varepsilon) = 2K_{eff}(\varepsilon)/M_s$ is the effective anisotropy field and Y_{Co} is Young's modulus of the Co.

Next, we fabricated devices (see Figs. 1(a) and 1(b)) in which a rectangular dot of Co/MgO/Ta was patterned at the center of a Ta/Pt cross-Hall bar.[29] All measurements were carried out at room temperature. As many as 10 devices were measured, and a very similar behavior was observed in all of the devices. An in-plane magnetic field (H_x) was applied along the current channel (within the accuracy of $1°$). For comparison, we measured two devices, one on the flexible PENC for the flat $(R = \infty$ or $\varepsilon = 0)$ condition and the other on the rigid and planar Si/SiO$_x$. Both devices have nominally identical structures: a current channel with $2\,\mu$m width, $t_{Co} \approx 1.0$ nm, and a rectangular dot of Co/MgO/Ta with a dimension of $2\,\mu\text{m} \times 6\,\mu\text{m}$ at the center. Fig. 1(c) shows an example of a magnetic hysteresis loop obtained from the flexible device. For this, the Hall resistance (r_H) is measured as a function of an applied out-of-plane field (H_z) for in-plane DC $(I_{dc}) = 0$ mA. Note that to ensure all the initial conditions are settled, Fig. 1(c) was measured after sweeping a large I_{dc} back and forth in the current channel a few times. After such sweeps, the magnetic hysteresis loops settle down to the one shown in Fig. 1(c) and does not change for further sweeps of current. We surmise that a substantial Joule heating on the PENC may modify the magnetic

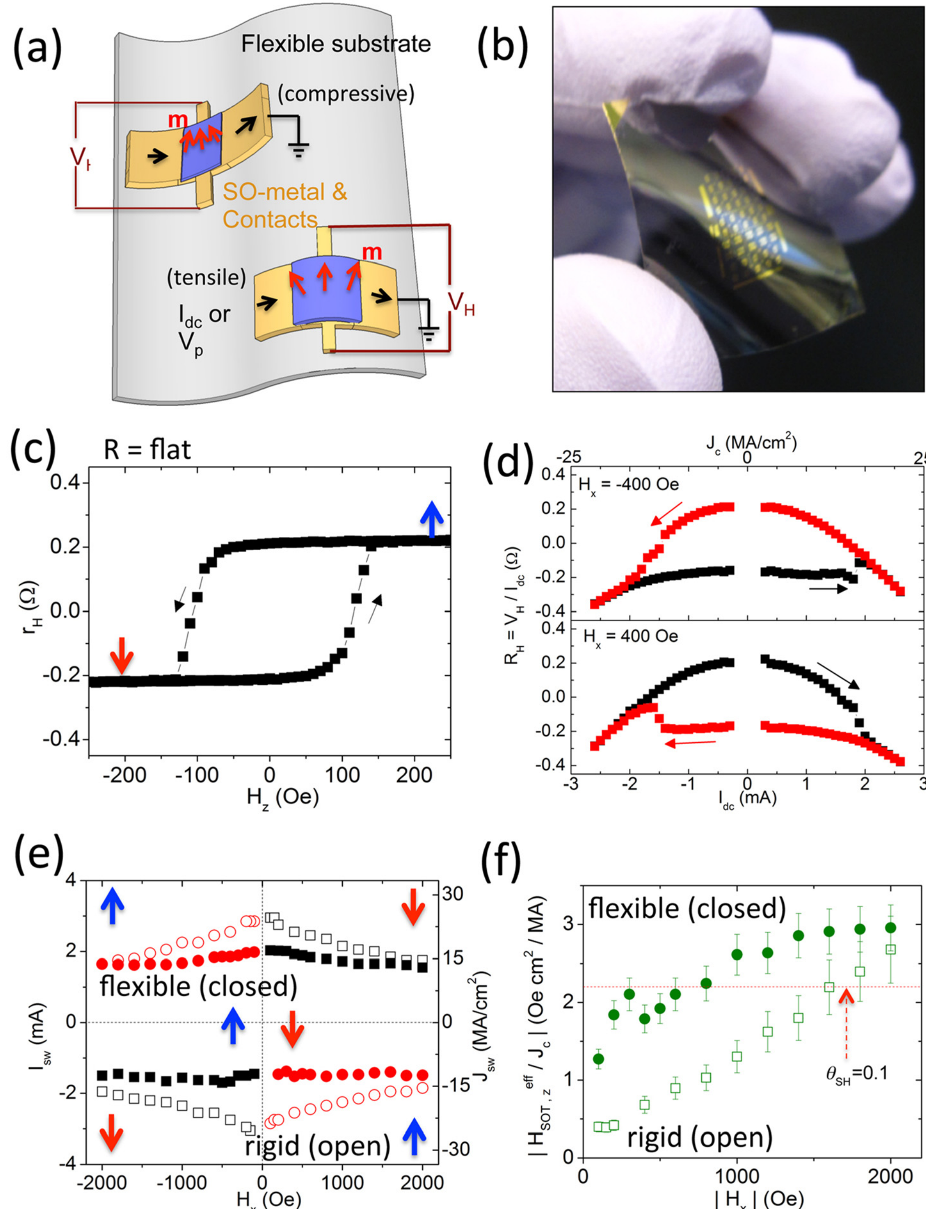

FIG. 1. Spin-orbit-torque (SOT) device on a flexible plastic substrate and electrical/magnetic characteristics for the flat $(R = \infty)$ condition. (a) Schematic of SOT-devices on a flexible plastic substrate. A Co/MgO/Ta rectangular dot is patterned at the center of a Ta/Pt cross bar. The SOT induced by in-plane dc currents (I_{dc}'s) or voltage pulses (V_p's) can drive a perpendicular magnetization reversal while the flexible device can be bent as a result having tensile or compressive strain. (b) Photograph of fabricated SOT-devices on the PENC substrate. (c)–(f), The results obtained from a flexible SOT device. (c) Hysteresis loop r_H vs H_z at $I_{dc} = 0$ mA for the flat $(\varepsilon = 0)$ condition after one I_{dc}-induced switching. (d) Examples of the current-induced deterministic switching in the presence of an in-plane external $H_x \approx \pm 400$ Oe for the flat condition. (e) Switching phase diagram (SPD) of the flexible SOT-device, showing the switching current (I_{sw}) as a function of H_x. To compare, this plot also shows the SPD of a rigid SOT-device on a thermally oxidized Si substrate (Si/SiO$_x$). Both devices had nominally identical structures. The SPDs summarize the bi-stable region and the switching direction under H_x and I_{dc}. (f) Estimated values of $|H_{SOT,z}^{eff}/J_c|$ as function of $|H_x|$ for both of the SOT-devices, obtained from the analysis of SPDs.[29] The redline presents the calculated $\theta_{SH} = 0.1$ for $M_s = 970\,\text{emu/cm}^3$ and $t_{Co} = 1$ nm.

profile, resulting from the glass transition of the plastic substrate if the enhanced $T > T_g$ ($\approx 120\,^\circ$C) at which the second order phase change of the plastic substrate occurs from a glassy state to a rubbery state.[28] In any case, from the hysteresis loop, a good PMA with an out-of-plane switching field $H_p \approx 110$ Oe is observed. This is very close to the H_p of the rigid device.[29]

Next, we explored the I_{dc}-induced switching of a Co/MgO/Ta dot on the flexible device in the absence of any bending ($R = \infty$). We obtained deterministic magnetic reversals of the Co layer between $m_z \approx +1$ (up) and $m_z \approx -1$ (down) in the presence of an external H_x that is collinear to the direction of I_{dc}. As illustrated in Fig. 1(d) for $H_x \approx \pm 400$ Oe, the magnetic reversals occur at the switching current ($|I_{sw}|$) ≈ 1.75 mA ($|J_{sw}| \approx 14.6$ MA/cm^2) from up to down if $I_{sw} \times H_x < 0$ and from down to up if $I_{sw} \times H_x > 0$. This "handedness" of the R_H–I_{dc} loop is a Hallmark signature of SOT induced switching.[12,16–19] Fig. 1(e) shows the switching phase diagram (SPD) for H_x and I_{sw}, summarizing the bi-stable region and the switching direction under H_x and I_{dc}. The switching symmetries are consistent with previously[12,16–20] observed SOT induced perpendicular magnetization switching for Pt/Co stacks and with the positive spin-Hall angle (θ_{SH}) of the underlying-Pt layer.

Notably, the flexible device had lower $|I_{sw}|$'s than the rigid device (see Fig. 1(e)) for low $|H_x|$'s. We postulate that one reason for this is more significant Joule-heating effect of the flexible device as the heat dissipation of the PENC is $\sim$8 times less efficient than it is through the Si/SiO$_x$.[29] There is also an indication that the Dzyaloshinskii-Moriya interaction (DMI)[18,20,21,30] for the material stack on the PENC is weaker than its counterpart on the Si/SiO$_x$, as implied in Fig. 1(f). Previous study[18] suggested that an external H_x is required for the complete switching because a preferred chirality in the domain wall (DW) of a nucleated sub-domain, set by the presence of DMI at the magnetic interface having a structural inversion asymmetry (SIA), should be broken and be aligned to H_x. Then, the anti-damping component of the SOT gives an effective out-of-plane field ($H^{eff}_{SOT,z} = \frac{\hbar}{\pi e}\frac{\theta_{SH}}{M_s t_{Co}} J_c \langle m_x \rangle$) on the wall that can provoke a thermally activated depinning of the wall and that can drive the nucleated domain expansion to the rest of the magnet and complete the magnetic switching. Here, m_x is in-plane component of the magnetization at the center of the wall and $\langle m_x \rangle$ is the averaged around the nucleated domain. Hence, a weaker DMI should lead to a smaller $|I_{sw}|$ for low $|H_x|$'s due to more orientation of the magnetization (m_x) within the pinned DW to the direction of H_x. A weaker DMI or a less interface effect of the flexible device might be expected, based on the magnetic reversal process, because the PENC has $\sim$1.5 times greater R_a than the Si/SiO$_x$ substrate.

Figure 1(f) plots the estimated $|H^{eff}_{SOT,z} / J_c|$ as a function of $|H_x|$ for both devices.[29] For the flexible device, the $|H^{eff}_{SOT,z}/J_c|$ saturated to $\sim$3Oe·cm^2/MA for $|H_x| > 1.3$–1.4 kOe. The saturation indicates that beyond this point, the $|H_x|$ was strong enough to overcome DW chirality set by the DMI[18] (i.e., $|m_x| \to 1$). Since the redline corresponded to the calculated θ_{SH}=0.1 for M_s=970emu/cm^3, t_{Co}=1nm, we had $\theta_{SH}\approx$0.13 for the flexible device at the saturations if there was no reduction of M_s. However, the actual θ_{SH} should be lower (to 50%–60%) since there was a significant reduction of M_s at an elevated T by Joule heat due to the nature of 2 dimensional characteristics of the ultrathin Co. In comparison, for the rigid device, the $|H^{eff}_{SOT,z}/J_c|$ kept increasing up to $|H_x|$=2kOe and did not show any tendency to saturate. This indicates that the DMI for the films on the rigid substrate was stronger compared to that on the flexible substrate. If $H_x\approx$1.3 kOe and$\approx$2.5 kOe was the field that fully overcame the DMI field ($H_D = D/M_s\delta_{DW}$) for the flexible device and for the rigid device, we obtained $D\approx -0.75$erg/cm^2 and -1.45erg/cm^2, respectively, after accounting the reduction of M_s.

Next, we examined the operational stability as a function of bending for the flexible devices. First, the channel resistance (R_c) was measured as a function of bend radius (R) or strain (ε); R (or ε) > 0 for tensile strain while R (or ε) < 0 for compressive strain. Figure 2(a) shows that the R_c increased (decreased) with a tensile (compressive) strain as expected, and overall the R_c was varied $\sim$2% from $R = 20$ mm ($\varepsilon \approx +0.3\%$) to -30 mm ($\varepsilon \approx -0.2\%$), i.e., $\Delta\varepsilon \approx 0.5\%$. We further measured the hysteresis loops r_H vs H_z at $I_{dc} = 0$ mA, for $R = \infty$ (flat), 20 mm or -30 mm. Figure 2(b) shows the $H_p \approx 150 \pm 5$ Oe for all of the bending conditions, indicating that the H_p was not sensitive to the specific bending conditions; any change in H_p was essentially within the error margin. Lastly, we measured the I_{dc}-induced magnetic reversals $H_x \approx \pm 500$ Oe, again for varying bending conditions. Figs. 3(c) and 3(d) illustrate the measured results in which the switching symmetries with I_{dc} and H_x are unchanged and that the I_{sw}'s remains unaffected.

We understand this robustness of the switching behaviors to the external ε due to the insensitivities of the θ_{SH} and H_k^{eff} to it. From the scattering theory[31,32] to generate the SOT, the θ_{SH} is proportional to the resistivity of Pt (ρ_{Pt}) for an intrinsic (band-structure) scattering mechanism while the θ_{SH} is independent of ρ_{Pt} for an extrinsic skew scattering mechanism. For any cases, 2% change of the R_c or ρ_{Pt} is too small to cause any significant change in the θ_{SH}. We also expect that the change in the effective anisotropy field, $\Delta H_k^{eff}(\varepsilon) = -3\lambda_{Co}Y_{Co}\varepsilon/M_s$, was about 140 Oe with $\varepsilon = 0.3\%$. This was still too small compared to the strong PMA of the flexible device with $t_{Co} = 1$ nm ($H_k^{eff} > 12$ kOe). However, we note that the details of the switching mechanism may change a little, as evidenced by the slight changes in the loops. Such changes are expected because domain nucleation and expansion processes might be slightly altered by stress and strain, which could be sensitive with a small field.

We further explored quasi-static switching by applying a pulse voltage train. The device used had a width of 5 μm, $t_{Co} \approx 0.8$ nm, and a perpendicularly magnetized Co/MgO/Ta dot having dimensions of 5 μm $\times$ 7 μm. Figure 3(a) shows the measured hysteresis loop r_H vs H_z for $R = \infty$, 20 mm or -30 mm. The width of the applied pulses is 10 ns, and its amplitude is modulated to mimic a voltage sweep (see Fig. 3(b)). Figures 3(c) and 3(d) show the quasi-static r_H–V_p loops for $H_x \approx \pm 500$ Oe for $R = \infty$, 20 mm or -30 mm. The corresponding loops show qualitatively similar behavior as the ones obtained with I_{dc}'s (see, for example, the difference between highest and lowest resistance values). Note that

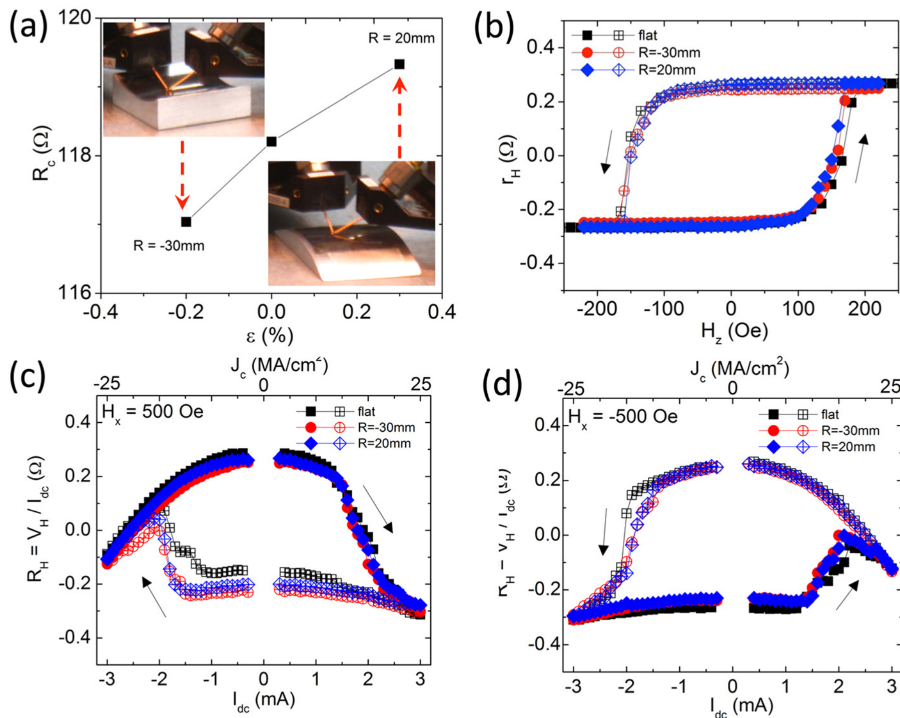

FIG. 2. Characteristics of a flexible SOT device ($t_{Co} \approx 1.0$ nm) with in-plane dc currents for flat, compressive, and tensile conditions. (a) Hysteresis loops of r_H as a function of H_z at $I_{dc} = 0$ mA for flat ($R = \infty$), tensile ($R = 20$ mm), and compressive ($R = -30$ mm) conditions. (b) Measured resistance of current channel (R_c) as a function of R. Inset photos: the flexible SOT device being bent during the measurements. (c) and (d) Hysteresis curves of $R_H = V_H / I_{dc}$ vs I_{dc} at $H_x = \pm 500$ Oe for $R = \infty$, 20 mm or -30 mm. The flexible SOT device was insensitive to the radius of curvature up to $|R| \approx \pm 20$–30 mm.

beyond $|V_p| \sim 2$ V, the magnet starts to respond to 10 ns pulses. Complete switching does not happen at this point due to the large size of the magnets used in this study, which eventually leads to domain nucleation and intermediate states between fully up and down. As the magnet size is reduced (e.g., ~200 nm in diameter), nano-second switching of the magnets can be achieved.[33] Finally, as it is with the I_{dc}'s, the loops do not show any appreciable change depending on the bending conditions, indicating the robustness of the devices against the applied ε. We note that the lower curvature in Figs. 3(c) and 3(d) was due to the dissipation of a heat during the current-off time, compared to the continuous dc current case in Figs. 2(c) and 2(d).

We also tested the endurance of the devices on the flexible substrate by measuring their behavior after the application of successive voltage pulses (V_p's). For this, 10^6 pulses with 10 ns pulse width were applied for $R = \infty$. The switching field ($H_p = (H_p^+ - H_p^-)/2$) and the full delta Hall resistance ($\Delta r_H = r_H$ ($m_z \approx +1$) $- r_H$ ($m_z \approx -1$)) were intermittently checked and compared with those obtained from r_H vs H_z loop at $I_{dc} = 0$ mA, as shown in Fig. 4(a). As observed in Fig. 4(b), H_p and Δr_H did not show any appreciable change after the application of 10^6 pulses, thus attesting to very high endurance of the fabricated devices.

In summary, we have shown the flexible plastic PENC as a suitable platform for implementing spintronic devices

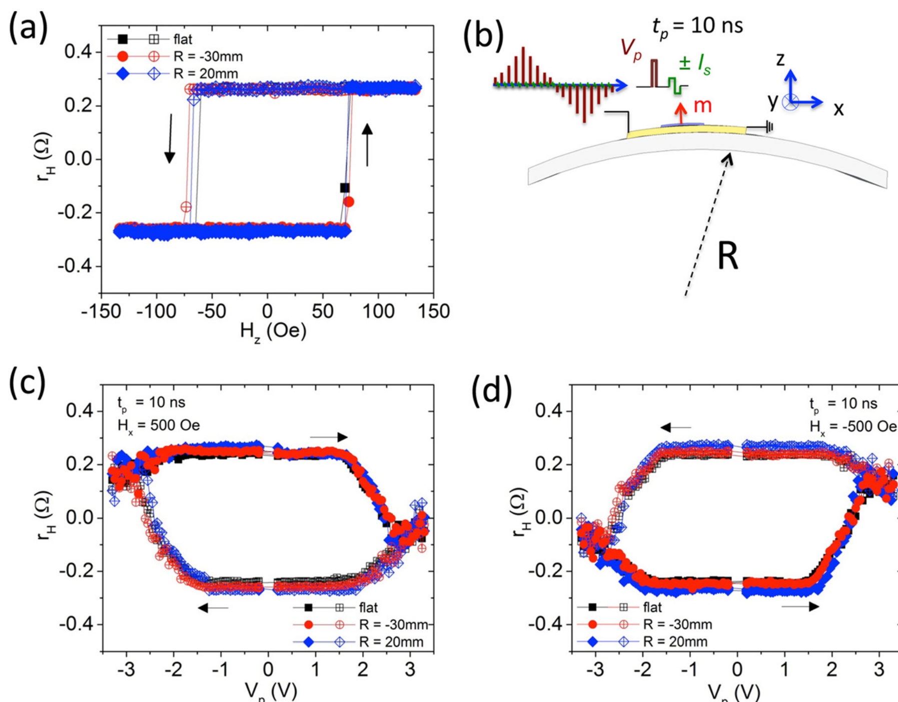

FIG. 3. Characteristics of a flexible SOT device ($t_{Co} \approx 0.8$ nm) with voltage pulses for flat, tensile, and compressive bent conditions. (a) Hysteresis loops of r_H vs H_z at $I_{dc} = 0$ mA for flat ($R = \infty$), tensile ($R = 20$ mm), or compressive ($R = -30$ mm) conditions. (b) Schematic of voltage pulse induced switching measurement. Small positive/negative sense currents ($\pm 5\,\mu$A) are applied between successive pulses for monitoring the perpendicular component of the Co magnetization. (c) and (d) Hysteresis curves of r_H as a function of V_p at $H_x = \pm 500$ Oe for $R = \infty$, 20 mm, or -30 mm. The flexible SOT device was insensitive to the radius of the curvature up to $|R| \approx \pm 20$–30 mm.

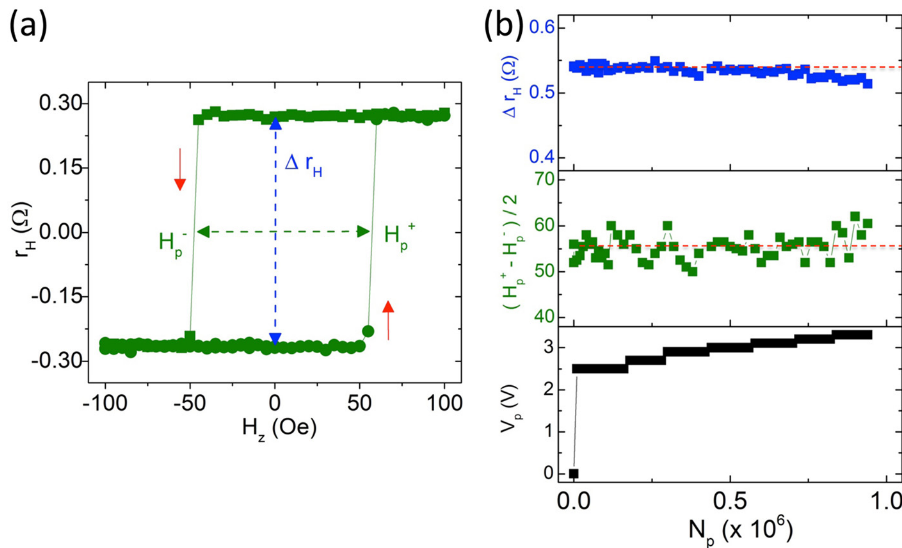

FIG. 4. Endurance test of the SOT device on the flexible plastic substrate. (a) Example of r_H vs H_z loop at $I_{dc} = 0$ mA. From this loop, we can obtain the switching field ($H_p = (H_p^+ - H_p^-)/2$) and the full delta Hall resistance ($\Delta r_H = r_H\ (m_z \approx +1) - r_H\ (m_z \approx -1)$). (b) Variations of measured H_p, Δr_H, and applied V_p as a function of number of pulses (N_p) up to $\sim 10^6$. We checked the magnetic stability of the SOT device with the variations of H_p and Δr_H.

where perpendicular magnetization can be suitably controlled using SOT generated by an in-plane current. This work demonstrates that magnetic hetero-structures with good interface qualities can be synthesized on the flexible organic substrate. Retention of such interface quality indicates that much more complex stacks could potentially be developed for many other types of devices on such substrates. The quasi-static switching and robust operation after a million pulses show that high performance and high endurance behavior, the significant advantages provided by magnetic materials (over competing material systems such as oxides), otherwise grown on rigid substrates, can be achieved on flexible platforms as well. While we have focused on the insensitivity to ε, it should be possible to grow magnetic materials with large λ where magnetic anisotropy, domain nucleation, and propagation will be significantly affected by strain and bending. This could provide innovative means to control and understand emerging phenomena in thin ferromagnets.[13]

The authors would like to thank Dominic Labanowski for useful conversations. This research was supported in part by the Center of Function Accelerated NanoMaterial Engineering (FAME), one of the six SRC STARnet Centers, sponsored by MARCO and DARPA; and the NSF E^{3}S center at Berkeley, Grant No. ECCS-0939514. The materials' development was funded by U.S. Department of Energy, Office of Science, Office of Basic Energy Sciences under Award No. DE-SC0012371.

[1]D. H. Kim, R. Ghaffari, N. Lu, and J. A. Rogers, Annu. Rev. Biomed. Eng. **14**, 113 (2012).
[2]J. Jang, F. Pan, K. Braam, and V. Subramanian, Adv. Mater. **24**, 3573 (2012).
[3]M. Melzer, M. Kaltenbrunner, D. Makarov, D. Karnaushenko, D. Karnaushenko, T. Sekitani, T. Someya, and O. G. Schmidt, Nat. Commun. **6**, 6080 (2015).
[4]J. A. Rogers, T. Someya, and Y. Huang, Science **327**, 1603 (2010).
[5]X. Zhang, Q. Zhan, G. Dai, Y. Liu, Z. Zuo, H. Yang, B. Chen, and R.-W. Li, J. Appl. Phys. **113**, 17A901 (2013).
[6]M. Gueye, B. M. Wague, F. Zighem, M. Belmeguenai, M. S. Gabor, T. Petrisor, Jr., C. Tiusan, S. Mercone, and D. Faurie, Appl. Phys. Lett. **105**, 062409 (2014).
[7]W. Che, X. Xiao, N. Sun, Y. Zhang, R. Shan, and Z. Zhu, Appl. Phys. Lett. **104**, 262404 (2014).
[8]Z. Tang, B. Wang, H. Yang, X. Xu, Y. Liu, D. Sun, L. Xia, Q. Zhan, B. Chen, M. Tang *et al.*, Appl. Phys. Lett. **105**, 103504 (2014).
[9]C. Barraud, C. Deranlot, P. Seneor, R. Mattana, B. Dlubak, S. Fusil, K. Bouzehouane, D. Deneuve, F. Petroff, and A. Fert, Appl. Phys. Lett. **96**, 072502 (2010).
[10]A. Bedoya-Pinto, M. Donolato, M. Gobbi, L. E. Hueso, and P. Vavassori, Appl. Phys. Lett. **104**, 062412 (2014).
[11]A. Brataas, A. D. Kent, and H. Ohno, Nat. Mater. **11**, 372–381 (2012).
[12]J. Sinova, S. O. Valenzuela, J. Wunderlich, C. H. Back, and T. Jungwirth, e-print arXiv:1411.3249.
[13]F. Matsukura, Y. Tokura, and H. Ohno, Nat. Nanotechnol. **10**, 209 (2015).
[14]N. Locatelli, V. Cros, and J. Grollier, Nat. Mater. **13**, 11–20 (2014).
[15]H.-S. Philip Wong and S. Salahuddin, Nat. Nanotechnol. **10**, 191 (2015).
[16]I. M. Miron, K. Garello, G. Gaudin, P. J. Zermatten, M. V. Costache, S. Auffret, S. Bandiera, B. Rodmacq, A. Schuhl, and P. Gambardella, Nature **476**, 189 (2011).
[17]L. Liu, O. J. Lee, T. J. Gudmundsen, D. C. Ralph, and R. A. Buhrman, Phys. Rev. Lett. **109**, 096602 (2012).
[18]O. J. Lee, L. Q. Liu, C. F. Pai, Y. Li, H. W. Tseng, P. G. Gowtham, J. P. Park, D. C. Ralph, and R. A. Buhrman, Phys. Rev. B **89**, 024418 (2014).
[19]L. Q. Liu, C.-F. Pai, Y. Li, H. W. Tseng, D. C. Ralph, and R. A. Buhrman, Science **336**, 555 (2012).
[20]S. Emori, U. Bauer, S. M. Ahn, E. Martinez, and G. S. D. Beach, Nat. Mater. **12**, 611 (2013).
[21]K.-S. Ryu, L. Thomas, S.-H. Yang, and S. Parkin, Nat. Nanotechnol. **8**, 527 (2013).
[22]L. You, O. J. Lee, D. Bhowmik, D. Labanowski, J. Hong, J. Bokor, and S. Salahuddin, Proc. Natl. Acad. Sci. U.S.A. **112**(33), 10310 (2015).
[23]J. Kim, J. Sinha, M. Hayashi, M. Yamanouchi, S. Fukami, T. Suzuki, S. Mitani, and H. Ohno, Nat. Mater. **12**, 240 (2013).
[24]G. Yu, P. Upadhyaya, Y. Fan, J. G. Alzate, W. Jiang, K. L. Wong, S. Takei, S. A. Bender, L.-T. Chang, Y. Jiang *et al.*, Nat. Nanotechnol. **9**, 548 (2014).
[25]X. Qiu, K. Narayanapillai, Y. Wu, P. Deorani, D.-H. Yang, W.-S. Noh, J.-H. Park, K.-J. Lee, H.-W. Lee, and H. Yang, Nat. Nanotechnol. **10**, 333 (2015).
[26]Z. Suo, E. Y. Ma, H. Gleskova, and S. Wagner, Appl. Phys. Lett. **74**, 1177 (1999).
[27]J. Noh, D. Yeom, C. Lim, H. Cha, J. Han, J. Kim, Y. Park, V. Subramanian, and G. Cho, IEEE Trans. Electron. Packag. Manuf. **33**(4), 275 (2010).
[28]W. A. MacDonald, M. K. Looney, D. MacKerron, R. Eveson, R. Adam, K. Hashimoto, and K. Rakos, J. Soc. Inf. Disp. **15**, 1075 (2007).
[29]See supplementary material at http://dx.doi.org/10.1063/1.4936934 for further information.
[30]A. Thiaville, S. Rohart, E. Jue, V. Cros, and A. Fert, Europhys. Lett. **100**, 57002 (2012).
[31]T. Tanaka, H. Kontani, M. Naito, T. Naito, D. S. Hirashima, K. Yamada, and J. Inoue, Phys. Rev. B **77**, 165117 (2008).
[32]N. Nagaosa, J. Sinova, S. Onoda, A. H. MacDonald, and N. P. Ong, Rev. Mod. Phys. **82**, 1539 (2010).
[33]K. Garello, C. O. Avci, I. M. Miron, M. Baumgartner, A. Ghosh, S. Auffret, O. Boulle, G. Gaudin, and P. Gambardella, Appl. Phys. Lett. **105**, 212402 (2014).